

RESEARCH ARTICLE

10.1002/2017JA024266

Key Points:

- Heavy planetary ion enhancements in Mercury's duskside current sheet provide explanation for cross-tail asymmetries found in this study
- The total current due to the pileup of magnetic flux and conductance required to close the SCW current is found to be almost equal to 11 kA and 1.2 S
- Mercury is coupled to magnetotail by mass loading of heavy ions and field-aligned currents driven by reconnection-related fast plasma flow

Correspondence to:

G. Poh,
gangkai@umich.edu

Citation:

Poh, G., J. A. Slavin, X. Jia, J. M. Raines, S. M. Imber, W.-J. Sun, D. J. Gershman, G. A. DiBraccio, K. J. Genestreti, and A. W. Smith (2017), Coupling between Mercury and its nightside magnetosphere: Cross-tail current sheet asymmetry and substorm current wedge formation, *J. Geophys. Res. Space Physics*, 122, 8419–8433, doi:10.1002/2017JA024266.

Received 14 APR 2017

Accepted 17 JUL 2017

Accepted article online 20 JUL 2017

Published online 19 AUG 2017

Coupling between Mercury and its nightside magnetosphere: Cross-tail current sheet asymmetry and substorm current wedge formation

Gangkai Poh¹ , James A. Slavin¹ , Xianzhe Jia¹ , Jim M. Raines¹ , Suzanne M. Imber² , Wei-Jie Sun^{3,4} , Daniel J. Gershman⁵ , Gina A. DiBraccio^{6,7} , Kevin J. Genestreti⁸ , and Andy W. Smith⁹ 

¹Department of Climate and Space Sciences and Engineering, University of Michigan, Ann Arbor, Michigan, USA,

²Department of Physics and Astronomy, University of Leicester, Leicester, UK, ³Key Laboratory of Earth and Planetary Physics, Institute of Geology and Geophysics, Chinese Academy of Sciences, Beijing, China, ⁴School of Earth and Space Sciences, Peking University, Beijing, China, ⁵Heliophysics Science Division, NASA Goddard Space Flight Center, Greenbelt, Maryland, USA, ⁶Solar System Exploration Division, NASA Goddard Space Flight Center, Greenbelt, Maryland, USA,

⁷Universities Space Research Association, Columbia, Maryland, USA, ⁸Space Science and Engineering Division, Southwest Research Institute, San Antonio, Texas, USA, ⁹Department of Physics and Astronomy, University of Southampton, Southampton, UK

Abstract We analyzed MErcury Surface, Space ENvironment, GEOchemistry, and Ranging (MESSENGER) magnetic field and plasma measurements taken during 319 crossings of Mercury's cross-tail current sheet. We found that the measured B_z in the current sheet is higher on the dawnside than the duskside by a factor of ≈ 3 and the asymmetry decreases with downtail distance. This result is consistent with expectations based upon MHD stress balance. The magnetic fields threading the more stretched current sheet in the duskside have a higher plasma beta than those on the dawnside, where they are less stretched. This asymmetric behavior is confirmed by mean current sheet thickness being greatest on the dawnside. We propose that heavy planetary ion (e.g., Na^+) enhancements in the duskside current sheet provides the most likely explanation for the dawn-dusk current sheet asymmetries. We also report the direct measurement of Mercury's substorm current wedge (SCW) formation and estimate the total current due to pileup of magnetic flux to be ≈ 11 kA. The conductance at the foot of the field lines required to close the SCW current is found to be ≈ 1.2 S, which is similar to earlier results derived from modeling of Mercury's Region 1 field-aligned currents. Hence, Mercury's regolith is sufficiently conductive for the current to flow radially then across the surface of Mercury's highly conductive iron core. Mercury appears to be closely coupled to its nightside magnetosphere by mass loading of upward flowing heavy planetary ions and electrostatically by field-aligned currents that transfer momentum and energy to the nightside auroral oval crust and interior. Heavy planetary ion enhancements in Mercury's duskside current sheet provide explanation for cross-tail asymmetries found in this study. The total current due to the pileup of magnetic flux and conductance required to close the SCW current is found to be ≈ 11 kA and 1.2 S. Mercury is coupled to magnetotail by mass loading of heavy ions and field-aligned currents driven by reconnection-related fast plasma flow.

1. Introduction

One of the major discoveries of the Mariner 10 mission was that Mercury possesses a global magnetic field, with dipole moment ≈ 100 times weaker than that of Earth's [Alexeev *et al.*, 2010; Anderson *et al.*, 2011]. The solar wind interaction with Mercury's largely dipolar magnetic field results in the formation of a smaller but more dynamic magnetosphere that is structurally similar to Earth's. Magnetic reconnection opens magnetic flux at Mercury's dayside magnetopause [Slavin *et al.*, 2009; DiBraccio *et al.*, 2013], which is then transported antisunward into the tail lobes. The northern and southern tail lobes contain sunward and antisunward magnetic fields, respectively; the central plasma sheet, which is a high plasma beta β (i.e., ratio of thermal pressure to magnetic pressure) region, divides the two lobes. Embedded within the plasma sheet is Mercury's cross-tail current sheet with the cross-tail current flowing from dawn to dusk of the magnetotail. As the cross-tail current thins to spatial scale of an ion inertial length, magnetic reconnection can occur.

In situ magnetic field and plasma measurements from MErcury Surface, Space ENvironment, GEochemistry, and Ranging (MESSENGER) have allowed large-scale statistical studies to be conducted to investigate the properties and dynamics of Mercury's cross-tail current sheet. *Poh et al.* [2017] identified a total of 319 current sheet crossings over 4 years of MESSENGER data and demonstrated that the time-averaged structure of Mercury's current sheet can be well represented by a Harris current sheet model [Harris, 1962]. By fitting each current sheet crossing to the Harris current sheet model, they calculated an average current sheet thickness of $\approx 0.39 R_M$, with a cross-tail current density of $\approx 92 \text{ nA/m}^2$. Note that studies of Earth's current sheet [e.g., *Petrakovich et al.*, 2011] have demonstrated that embedded structures (i.e., current sheets with non-Harris-type profiles) are ubiquitous in the terrestrial current sheet. The question of whether Mercury's cross-tail current sheet is as highly structured on smaller spatial scales as Earth could not be answered until high time resolution and multipoint measurements become available at Mercury.

Analysis of plasma measurements by *Poh et al.* [2017] also suggests that contributions from heavy ions and proton temperature anisotropy are important in maintaining stress balance with Mercury's central plasma sheet. *Raines et al.* [2013] and *Gershman et al.* [2014] investigated the ion properties of Mercury's plasma sheet and found significantly higher Na^+ density in the premidnight region of the plasma sheet. The dawn-dusk asymmetry of Na^+ density in Mercury's plasma sheet is also observed in simulations by *Delcourt* [2013]. They demonstrated that heavy ions (e.g., Na^+ , O^+ , and Ca^+) of planetary origin can undergo a Speiser-type motion and accelerated preferentially into Mercury's duskside plasma sheet. It appears that Mercury is coupled to its nightside magnetotail through mass transport of heavy planetary ions, which results in the observed dawn-dusk asymmetry. Such coupling has been observed at other planetary magnetosphere (e.g., transport of ionospheric oxygen ions between Earth's ionosphere and plasma sheet). To understand the effect of this mass coupling process at Mercury, it is important that we characterize and investigate other cross-tail asymmetries in Mercury's magnetotail.

Dawn-dusk asymmetry is a ubiquitous phenomenon in planetary magnetotails. The availability of in situ magnetic field and plasma measurements from heliophysics and planetary missions has allowed us to conduct large-scale statistical studies to characterize the dawn-dusk asymmetries of magnetotail properties in terrestrial (see *Walsh et al.* [2017] for a complete review of cross-tail asymmetries at Earth) and the outer planet magnetotails, such as Jupiter and Saturn [e.g., *Bunce and Cowley*, 2001; *Arridge et al.*, 2015; *Smith et al.*, 2016], where the asymmetries are driven by internal plasma dynamics. Asymmetries in the properties of the plasma sheet have been most extensively studied at Earth due to the availability of multipoint measurements. *Fairfield et al.* [1981] first reported observation of asymmetry in the properties of Earth's plasma sheet using IMP 6, IMP 7, and IMP 8 data. Subsequently, *Slavin et al.* [1985] reported ISEE 3 observation of higher B_z (i.e., north-south component of magnetic field) by $\approx 1 \text{ nT}$ in the near-Earth ($|X| < 100 R_E$) dawnside plasma sheet. More recent studies using Geotail [*Wang et al.*, 2004; *Vasko et al.*, 2015] have confirmed these asymmetries in B_z and current sheet thickness in the terrestrial magnetotail. The magnitude of B_z is an indicator of the magnetic field geometry of the current sheet. A stronger B_z indicates a less stretched, thicker current sheet, while a weaker B_z indicates a more stretched, thinner current sheet. This asymmetry in current sheet thickness was also been observed by Active Magnetospheric Particle Tracer Explorers/Ion Release Module [*Baumjohann et al.*, 1990] and, more recently, Cluster [*Artemyev et al.*, 2011; *Rong et al.*, 2011].

Since thin current sheets are closely associated with the onset of magnetic reconnection, a thinner duskside magnetotail current sheet suggests that reconnection may occur more frequently on the duskside than dawnside current sheet. Recent studies on the location of magnetotail reconnection sites at Earth [*Nagai et al.*, 2013; *Genestreti et al.*, 2014] show that reconnection sites tend to occur on the duskside of the current layer for the entire solar cycle. The occurrence of magnetic structures that formed as a result of magnetotail reconnection, such as flux ropes, traveling compression regions [*Imber et al.*, 2011], and dipolarization fronts [*Liu et al.*, 2013], is also found to have similar dawn-dusk asymmetries with higher occurrence rate on the duskside current sheet. Oxygen ions were also observed to have higher density on the duskside of Earth's plasma sheet, which coincides with region of higher reconnection rate. The effects of heavy ions (in particular O^+ at Earth) have on magnetic reconnection is still an active area of research and debate within the terrestrial magnetosphere community. A natural question would be the following: what effects do the dawn-dusk asymmetry of heavy planetary ions in Mercury's plasma sheet have on magnetic reconnection?

Magnetic reconnection is the dominant plasma process that transfers momentum and energy into Mercury's inner tail region by converting stored magnetic energy in the tail lobe into kinetic energy of the plasma in the plasma sheet. High reconnection rates at Mercury's magnetopause [Slavin and Holzer, 1979; Slavin et al., 2009; DiBraccio et al., 2013] increase the overall energy in Mercury's magnetotail by loading it with magnetic flux. Observations of dipolarization [Sundberg et al., 2012], substorms activity [Slavin et al., 2010; Sun et al., 2015], and plasmoids [DiBraccio et al., 2015a; Sun et al., 2016] support the idea of rapid dissipation of magnetic energy in the tail through magnetic reconnection. Magnetotail reconnection sends newly reconnected closed (i.e., connected to Mercury) and open (i.e., connected to solar wind) magnetic field lines planetward and tailward of the reconnection X line, respectively. At Earth, these newly reconnected closed field lines embedded in high-speed bursty bulk flows (BBFs) brake as they encounter the stronger magnetic fields and higher plasma pressures found in the inner magnetosphere [Baumjohann et al., 1999]. The aggregate effect of multiple BBFs braking and pressure gradient associated with the flow diversion generates perpendicular and field-aligned currents that flow opposite to the cross-tail current (i.e., dusk to dawn) and upward (downward) on the dawnside (duskside) of the braking region. The perpendicular and field-aligned currents close through Earth's ionosphere, leading to the formation of the terrestrial substorm current wedge (SCW) and the onset of the auroral substorm [Hesse and Birn, 1991; Shiokawa et al., 1998; Baumjohann et al., 1999]. Earlier observations of substorm activity [Slavin et al., 2010; Sun et al., 2016] indicate that Mercury is electrodynamically coupled to its magnetotail through field-aligned currents in the manner similar to Earth. However, to date, no direct measurement of Mercury's substorm current wedge formation has been made.

This paper aims to investigate mass, momentum, and energy coupling between Mercury and its nightside magnetosphere by studying Mercury's cross-tail current sheet asymmetries and the formation of Mercury's substorm current wedge. The paper is organized as follows. In the next section, we summarize the structure of Mercury's cross-tail current sheet and present the results of case studies of dynamics in Mercury's current sheet. In section 3, we present the results of statistical analyses performed to identify asymmetries of current sheet properties and report the first direct observation of Mercury's substorm current wedge. In section 4, we discuss possible explanations for the observed magnetotail asymmetries, the nature of Mercury's substorm current wedge, and further implications of our results.

2. MESSENGER Instrumentation and Event Selection

In this study, we utilize the full-resolution magnetic field and plasma data from MESSENGER's Magnetometer (MAG) (20 vectors per second) [Anderson et al., 2007] and Fast Imaging Plasma Spectrometer (FIPS) (one energy scan per 10 s) [Andrews et al., 2007], respectively. The coordinate system used in our analysis is the aberrated Mercury solar magnetospheric (MSM') coordinate system. The MSM system is centered on Mercury's offset internal dipole with the X axis oriented sunward along the Sun-Mercury line, the Z axis parallel to the planetary spin axis and positive in the northward direction, and the Y axis completing the right-handed system. We rotate the MSM X and Y axes to account for solar wind aberration such that X'_{MSM} is opposite to the mean solar wind velocity vector; the rotation angle was calculated daily by assuming a radial solar wind with constant speed of 400 km/s.

In this work, we utilized the 319 current sheet crossing events identified in Poh et al. [2017] (hereafter referred to as Poh17) to perform the statistical dawn-dusk asymmetry analysis. To characterize the properties of Mercury's current sheet, Poh17 fitted the magnetic field measurements of each current sheet crossing to the one-dimensional Harris current sheet [Harris, 1962] model using a reduced least squares method. The relationship between B_X and Z'_{MSM} is given by

$$B_X(Z'_{MSM}) = B_0 \tanh\left(\frac{Z'_{MSM} - z_0}{L}\right) \quad (1)$$

where B_0 is the asymptotic lobe field, z_0 is the north-south position of the current sheet (CS) center, and L is the characteristic half-thickness of the CS. The corresponding equation for the cross-tail current density (J_Y) is given by

$$J_Y(Z'_{MSM}) = \frac{B_0}{\mu_0 L} \operatorname{sech}^2\left(\frac{Z'_{MSM} - z_0}{L}\right) \quad (2)$$

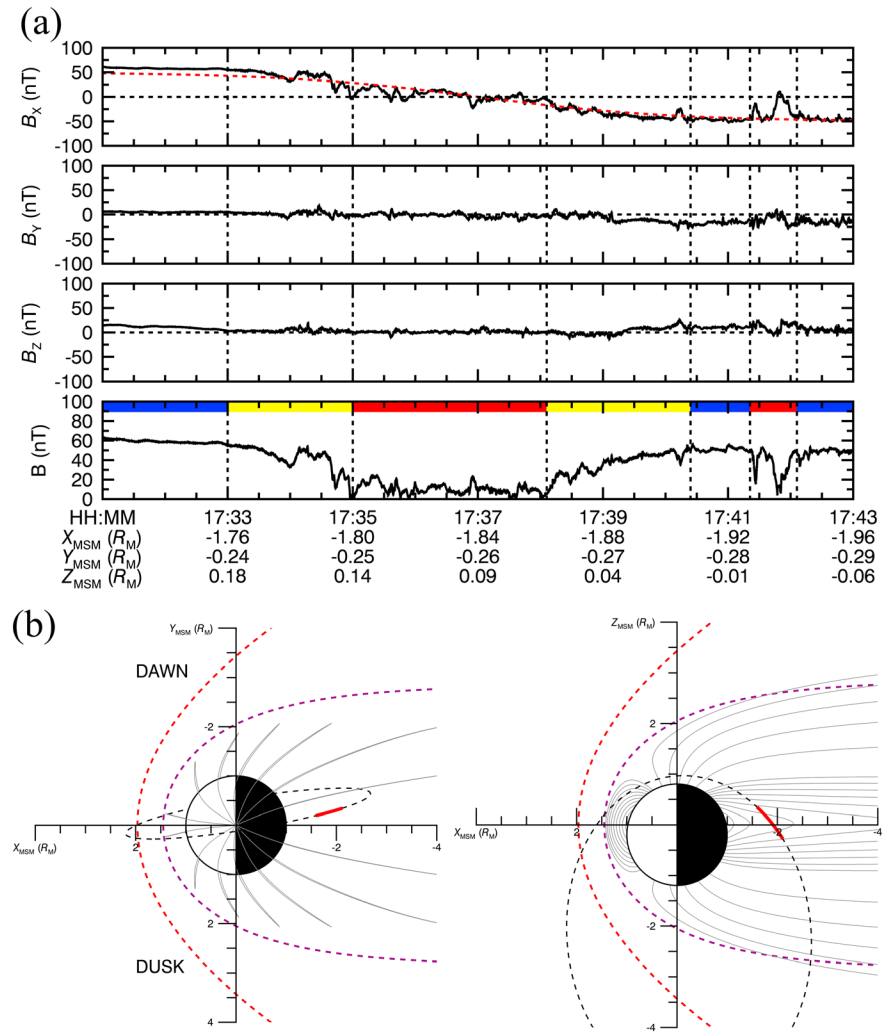


Figure 1. (a) Full-resolution magnetic field measurements of an example MESSENGER orbit on 28 August 2013 in aberrated Mercury solar magnetic (MSM) coordinates. The dotted lines and color bars separate each region of Mercury’s magnetotail, with blue, yellow, and red color bars representing the northern/southern tail lobe, plasma sheet boundary layer, and current sheet, respectively. (b) The orbit of MESSENGER on 28 August 2013 in the equatorial (left) and meridional (right) planes. The model bow shock (BS) and magnetopause (MP) from Winslow *et al.* [2013], scaled to fit observed average boundary crossings, are shown in dotted lines; the Sun is to the left, and the scaled T96 model magnetic field lines [Tsyganenko, 1995] using a linear scaling factor of 8 is shown in gray solid lines. Red line indicates the interval when MESSENGER traversed Mercury’s current sheet.

B_0 , z_0 , and L are the three free parameters in the reduced least squares fitting procedure of the Harris model to the B_x magnetic field measurements. We optimized the free parameters for each current sheet crossing fitting by minimizing the normalized value χ^2 given by

$$\chi^2 = \frac{1}{N} \sum_{i=0}^N (B_x^i - B_x^{\text{Model}})^2 \quad (3)$$

where N is the number of B_x measurement in each current sheet crossing and B_x^{Model} is given by equation (1). A normalized χ^2 value of 0.01 was set as the criterion for goodness of fit. Their results showed that $\approx 73\%$ of the 319 cross-tail current sheet crossings have $\chi^2 \leq 0.01$, which suggests that the long-wavelength structure of Mercury’s current sheet is well-represented by a Harris-type current sheet. The reader is referred to Poh17 for more details on the Harris current sheet fitting procedure.

MESSENGER’s magnetic field observations in Mercury’s cross-tail CS traversal on 28 August 2013 are shown in Figure 1a. The normalized χ^2 value of this reduced least squares fitting is ≈ 0.003 , and the Harris current sheet

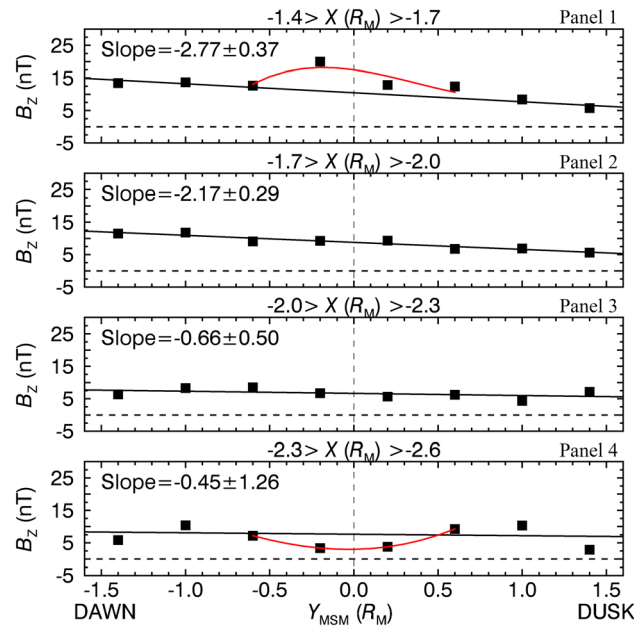


Figure 2. Plot of B_Z as a function of X'_{MSM} and Y'_{MSM} . B_Z is binned into four downtail distance from $X'_{MSM} = -1.4 R_M$ to $-2.6 R_M$ at bins of $0.3 R_M$ and dawn-dusk direction from $Y'_{MSM} = -1.6 R_M$ to $1.6 R_M$ at bins of $0.4 R_M$. Gray dashed lines mark the midnight meridian. The strength of the dawn-dusk asymmetry in each downtail distance is determined by the slope of linear least squares fitted lines (black). Red lines are the least squares polynomial fits for closest (i.e., $-1.4 R_M > X'_{MSM} > -1.7 R_M$) and farthest (i.e., $-2.3 R_M > X'_{MSM} > -2.6 R_M$), which represents the magnetic flux pileup and enhanced reconnection region, respectively.

[Rong et al., 2015], Mars [DiBraccio et al., 2015b, 2017], and Mercury [Poh et al., 2017]). Figure 1b shows MESSENGER's trajectory (red line) on 28 August 2013 in the equatorial (i.e., $X'_{MSM}-Y'_{MSM}$) and meridional (i.e., $X'_{MSM}-Z'_{MSM}$) plane. As a reference, the model bow shock (BS) and magnetopause (MP) [Winslow et al., 2013] are shown as red and purple dotted lines, respectively. The model magnetic field lines, shown as gray solid lines, are calculated using the T96 magnetic field model for Earth [Tsyganenko, 1995] and scaled with a linear scaling factor of 8.

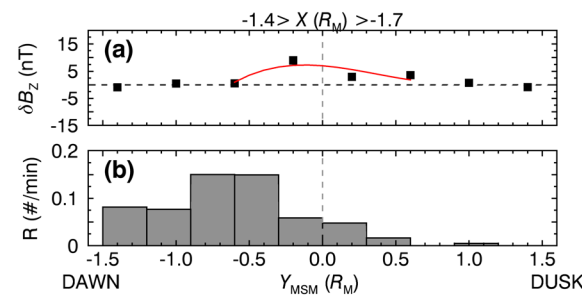


Figure 3. (a) Plot of δB_Z as a function of Y'_{MSM} for the downtail distance X'_{MSM} between $-1.4 R_M$ to $-1.7 R_M$. δB_Z is calculated by detrending B_Z values in Figure 2 (first panel) with the linear least squares fitted line (black). The plot format is similar to Figure 2. The detrended B_Z values are calculated by subtracting B_Z values with the "baseline values," which is determined from the least squares fitted line in panel 1 of Figure 2. The red line shows the persistent asymmetry of flux pileup in the substorm current wedge after subtraction of baseline values. (b) Distribution of occurrence rate (in number per minute) of dipolarization fronts observed by MESSENGER [Sun et al. 2016].

fitting result (red) is shown in the top panel of Figure 1a. The interval begins with MESSENGER in the northern tail lobe as shown by the blue bar, where $B_{X'}$ > 0 and $|\mathbf{B}|$ is constant at ≈ 60 nT. The spacecraft then encounters the plasma sheet boundary layer at $\sim 17:33$ UT, where $|\mathbf{B}|$ decreases by ≈ 20 nT and fluctuates with amplitudes of $\approx \pm 10$ nT. MESSENGER enters the central plasma sheet at 17:35 UT before crossing the embedded current sheet (i.e., $B_{X'}$ reverses polarity) at $\sim 17:37$ UT and exits into the southern tail lobe ($B_{X'} < 0$). MESSENGER also observed short-wavelength decreases in $|\mathbf{B}|$ with corresponding increases in $B_{X'}$ (i.e., "reencountering" of the current sheet in short time scale) when the spacecraft is deep in the southern tail lobe. These magnetic field signatures are typical of a transient magnetotail process known as tail flapping, where the magnetotail moves in the north-south direction relative to the spacecraft. It is a common phenomenon observed in Earth's [Volwerk et al., 2013] and other planetary magnetotail (e.g., Venus

3. Analysis

3.1. Cross-Tail Variation of B_Z

From the current sheet crossings identified by Poh17, we examined the variation of the z component of the central plasma sheet magnetic field (i.e., B_Z) as a function of cross-tail distance (i.e., Y'_{MSM}). Figure 2 is derived by binning all measurements based on MESSENGER's orbital coverage. The X'_{MSM} component ranges from -1.4 to $-2.6 R_M$ and has been divided into four intervals of $0.3 R_M$, while Y'_{MSM} ranges between -1.6 and $1.6 R_M$ and has been separated into eight intervals of $0.4 R_M$. Note that the error bar for each point represents the standard error of data points in each bin and

is magnified by 100 times in Figure 2 for clarity. Figure 2 shows two important magnetic field features of Mercury's current sheet:

1. A significant dawn-dusk asymmetry of varying degrees in B_Z is identified, where B_Z is higher at the dawnside than duskside of the current sheet and the strength of the asymmetry decreases with downtail distances. Figure 2 (first panel) shows that the dawnside B_Z (≈ 15 nT) is 3 times larger than the duskside B_Z (≈ 5 nT) in the region closest to Mercury (i.e., $-1.4 < X'_{\text{MSM}}(R_M) < -1.7$). As the downtail distance increases (Figure 2, second and third panels), the dawn-dusk difference in B_Z decreases (i.e., ≈ 7.5 nT and 2.5 nT, respectively) with the dawnside B_Z magnitude greater than the duskside. Figure 2 (fourth panel) shows no distinct dawn-dusk B_Z asymmetry feature in the region farthest from Mercury (i.e., $-2.3 < X'_{\text{MSM}}(R_M) < -2.6$). The decrease in the degree of asymmetry is also evident from the decreasing negative slope of the least squares linear fit (black line) from 2.77 to 0.45. This type of dawn-dusk asymmetry has also been observed and studied at Earth [Slavin *et al.*, 1985; Wang *et al.*, 2004; Vasko *et al.*, 2015]; however, the asymmetry is stronger at Mercury as compared to Earth and explanation for this phenomenon will be discussed in section 4.2.
2. Our analysis suggests the direct measurement of substorm current wedge formation in Mercury's magnetotail. Apart from the dawn-dusk asymmetry, Figure 2 (first panel) shows a further increase in B_Z by ≈ 10 nT around the midnight meridian. We fitted the values of B_Z between $Y'_{\text{MSM}} = \pm 0.8 R_M$ to a cubic polynomial to obtain an observed dawn-dusk profile of the B_Z increase, as shown by the red line in Figure 2 (first panel). We believe that this increase in B_Z is due to the pileup of magnetic flux as the planetward convecting magnetic field lines, from a reconnection X line farther downtail, brake into the stronger near-Mercury magnetic field. Such process is analogous to the formation of a SCW at Earth [McPherron *et al.*, 1973; Kepko *et al.*, 2015]. Consequently, we observe a weak decrease in B_Z (red line) by ≈ 5 nT, due to enhanced reconnection occurring, near the midnight meridian in the downtail region of $-2.3 < X'_{\text{MSM}}(R_M) < -2.6$ (Figure 2, fourth panel). Our results also demonstrate that the pileup region of magnetic flux is not centered on the midnight meridian; rather, the peak increase in B_Z occurs at $Y'_{\text{MSM}} \approx -0.2 R_M$ (i.e., shifted toward postmidnight current sheet). This indicates that more magnetic flux is being piled up dawnside than duskside, suggesting dawn-dusk asymmetry in tail reconnection. To determine whether this asymmetric preference of flux pileup is a real feature, we remove the magnetic field contributions in the Y'_{MSM} directions from both Mercury's planetary dipole field and the cross-tail current sheet by subtracting the B_Z values in Figure 2 (first panel) with the asymmetric baseline values determined from the least squares fitted line (black). As shown in Figure 3a, the remaining magnetic field perturbation δB_Z due to Mercury's substorm current wedge is plotted as a function of Y'_{MSM} . Our analysis shows a persistent dawn-dusk asymmetry in the amount of flux pileup in the near-Mercury current sheet. The occurrence rate of dipolarization fronts identified by Sun *et al.* [2016] is plotted in Figure 3b. It shows a peak in occurrence of dipolarization fronts in the dawnside current sheet, which coincides with our observed peak in magnetic flux pileup. Implications of this result will be discussed in section 4.2.

3.2. Plasma Beta β

We also examined the dawn-dusk variation in the proton plasma beta β_{CS} across the current sheet. The current sheet β_{CS} can be calculated using the proton (H^+) measurements from the FIPS instrument. However, the viewing geometry of the FIPS instrument during the current sheet crossings does not allow the instrument to observe a full phase space distribution function. By assuming subsonic flow in the current sheet and integrating several H^+ measurements into one measurement of plasma parameters, we can calculate the average β_{CS} for each current sheet crossing [Raines *et al.*, 2013; Gershman *et al.*, 2014]. We can also estimate β_{CS} in the current sheet using the magnetic field measurements. In our estimation of β_{CS} in the current sheet, we assumed constant isotropic plasma pressure throughout the current sheet and ignore contributions from electrons and pressure anisotropy effects. Magnetotail studies at Earth [e.g., Artemyev *et al.*, 2016] and Mercury [Poh *et al.*, 2017] have shown that anisotropy effects are important in the stress balance of the magnetotail. Hot ions moving along magnetic field lines in nongyrotronic orbits can result in anisotropic pressure with the off-diagonal term in the pressure tensor being zero (i.e., $p_{xz} \neq 0$) [e.g., Pritchett and Coroniti, 1992]. However, the ability to quantify the anisotropic pressure effect and electron pressure at Mercury is limited by the field of view of the plasma instrument's accommodation on MESSENGER. Therefore, we simply

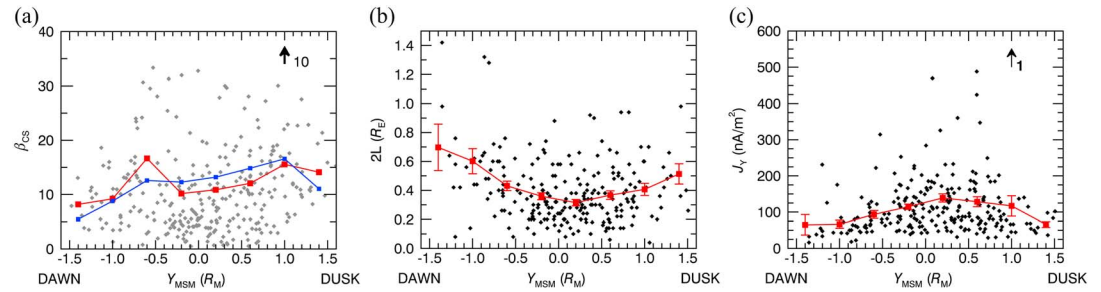


Figure 4. (a) Dawn-dusk distribution of current sheet plasma beta β_{CS} as shown by gray data points determined from the FIPS (red) and MAG (blue) instrument. (b) Current sheet full thickness $2L$ and (c) cross-tail current density J_Y of 234 current sheet crossings determined from the Harris current sheet model fitting. Data points are separated into bin size of $0.4 R_M$. The error bars represent the standard error of the mean for each bin and is given by $\text{std error} = \frac{\sigma}{\sqrt{N}}$ where σ and N is the standard deviation and total number of the data points in each bins, respectively. For both derived parameters, the data points (black) were binned into bins of $0.4 R_M$ between $Y_{MSM} = -1.6 R_M$ and $1.6 R_M$ as shown by the red data points. The error bars represent the standard error of the mean in each bin.

assume isotropic vertical pressure balance between the tail lobe magnetic pressure and the total pressure in the current sheet to derive the following equation [DiBraccio et al., 2013]:

$$\beta_{CS} = \left(\frac{B_{Lobe}}{B_{CS}} \right)^2 - 1 \tag{4}$$

where B_{Lobe} and B_{CS} are the mean magnetic field magnitude of the tail lobe and current sheet, respectively. The β_{CS} calculated using both methods outlined above are plotted as a function of the mean Y_{MSM} position in Figure 4a. Both methods of calculating β_{CS} using FIPS (red) and magnetic field (blue) measurements independently show good general agreement, hence lending confidence to the use of magnetic field-derived β_{CS} as proxy while plasma measurements are not available.

Figure 4a also shows dawn-dusk asymmetry in β_{CS} with the asymmetry being in an opposite sense as B_Z (i.e., β_{CS} is higher on the duskside current sheet than the dawnside). Note that the asymmetry of β_{CS} calculated from MAG is more obvious than that calculated from FIPS. The β_{CS} values calculated from FIPS proton measurements in this study are lower than the true value of β_{CS} since we only use the proton plasma pressure and did not include plasma pressure contribution from the heavy ions (e.g., Na^+). The asymmetry of heavy ions toward duskside of the current sheet, combined with their significant densities [Gershman et al., 2014], will affect the true measure of plasma beta in Mercury's plasma sheet. From the magnetohydrodynamics (MHD) stress balance equation ($\mathbf{J} \times \mathbf{B} = \nabla P$), as the plasma pressure increases, the tailward pressure gradient force also increases, hence stretching the magnetic field lines. B_Z decreases as the magnetic field lines are stretched and the current sheet is thinned. Therefore, our results are consistent with that expected from the MHD stress balance and show the inverse relationship between B_Z and β_{CS} . Consequently, our statistical results on B_Z and β_{CS} are consistent with the current sheet being thinner on the duskside than dawnside (i.e., dawn-dusk asymmetry similar to B_Z).

3.3. Current Sheet Thickness and Current Density

We also investigated the dawn-dusk asymmetry in the current sheet thickness d and current density J_Y using the Harris current sheet model fitting results determined by Poh17. Figure 4b shows the dawn-dusk distribution of the full current sheet thickness calculated from the Harris CS model fitting of the 234 selected events that satisfy the criteria of $\chi^2 \leq 0.01$. Our results also show a dawn-dusk asymmetry in the current sheet thickness with the duskside current sheet ≈ 10 – 30% thinner than the dawnside, thus supporting our earlier B_Z and β_{CS} asymmetry results. This is also consistent with earlier Earth's magnetotail studies, which found evidence of a thinner current sheet on the duskside of the terrestrial magnetotail [Artemyev et al., 2011; Rong et al., 2011]. Furthermore, our result shows that the current sheet is thicker on the flanks than the noon-midnight center of the magnetotail. The average current sheet thickness is $\approx 0.3 R_M$ around the midnight region and grows to $\approx 0.7 R_M$ and $0.5 R_M$ toward the dawnside and duskside current sheets, respectively. This result is also consistent with Earth's magnetotail observations [Fairfield, 1979; Slavin et al., 1985; Vasko et al., 2015].

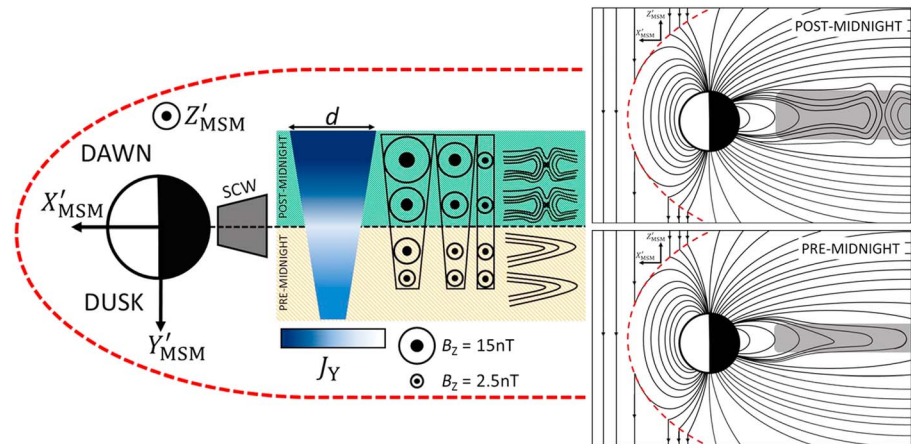


Figure 5. Schematic illustrations of summary and explanation for all asymmetries in Mercury's current sheet observed in this study. Red dashed line represents the magnetopause. Top and bottom panels on the right represent the postmidnight (dawn) and premidnight (dusk) views, respectively. The illustration shows that Mercury's current sheet is thicker and B_z is higher on the postmidnight than the premidnight region. The asymmetry in B_z also decreases in strength with increasing downtail distances. Mass loading of ions from the cusp and NMNL farther downtail drift stretches the duskside current sheet, while a dawnward preference in reconnection occurrence sends more dipolarized flux tube toward the dawnside current sheet and thereby thickening the current sheet. This difference in stretching and thickening of the current sheet may explain the dawn-dusk asymmetries observed in this study. Our results also strongly suggest the formation of a substorm current wedge in the near-Mercury region as shown in the diagram on the left. A dawnward preference in reconnection could also explain the observed asymmetric nature of the SCW.

Since MESSENGER is not a multispacecraft mission, and it does not have high time resolution plasma ion and electron distribution function measurements, we could not independently calculate the cross-tail current density in Mercury's magnetotail. However, the Harris CS modeling allows us to estimate the average current density J_Y as shown in Figure 4c. There is an opposite dawn-dusk asymmetry in J_Y as the thicker duskside current sheet has a higher average current density than the thinner dawnside current sheet. The cross-tail current density result is consistent with our earlier results of B_z and current sheet thickness since thinner current sheet produces higher current density for a given lobe field, as demonstrated in equation (1).

4. Discussion

MESSENGER observations of 319 current sheet crossings were examined with statistical analysis and model fitting. Our results can be summarized as follows:

1. A dawn-dusk asymmetry in B_z , β_{CS} , and current sheet thickness, d , is observed; B_z , β_{CS} , and d are lower, higher, and thinner, respectively, on the duskside than dawnside current sheets.
2. An enhancement in B_z in the nearest downtail region provides tentative evidence of Mercury's substorm current wedge.

4.1. Mercury's Asymmetric Cross-Tail Current Sheet

Our statistical analysis shows that B_z magnitude in the cross-tail current sheet sunward of the Near-Mercury Neutral Line (NMNL) is higher on the duskside than the dawnside. Furthermore, the strength of the asymmetry decreases with increasing downtail distance. Plasma beta, β_{CS} , and the thickness of Mercury's current sheet are also observed to have an opposite and similar dawn-dusk asymmetries as B_z , respectively. Consistent with MHD stress balance, higher plasma pressure (i.e., higher β_{CS}) stretches the current sheet magnetic field lines more, resulting in weaker B_z and a thinner current sheet. A summary illustration of the asymmetries observed in this study is shown in Figure 5. Magnetotail asymmetries have also been observed and studied extensively at Earth [e.g., Walsh et al., 2017]. With ISEE 3 and Geotail data, B_z in Earth's magnetotail is observed to have higher field strength at dawn than dusk [Slavin et al., 1985; Wang et al., 2004] and the plasma sheet is observed to be thicker on the dawnside than the duskside [Artemyev et al., 2011; Rong et al., 2011]. The stark similarities in magnetotail asymmetries between Earth and Mercury beg the question of whether the cause of Mercury's magnetotail asymmetry is similar to that of Earth's.

At Earth, the ionosphere is a significant source of O^+ and the contribution of O^+ to the total plasma sheet was observed to maximize on the duskside of the tail [Peterson *et al.*, 1981; Ohtani *et al.*, 2011]. Mercury's plasma sheet was observed to consist of primarily H^+ and Na^+ , with a similar premidnight-oriented asymmetry in the observed Na^+ density [Raines *et al.*, 2013; Gershman *et al.*, 2014]. Note that O^+ is observed only as a minor species in Mercury's plasma sheet. Even though the observed density of Na^+ in Mercury's plasma sheet is smaller than H^+ by a factor of 10 [Gershman *et al.*, 2014], the mass density of Na^+ is comparable to the H^+ because Na^+ is 23 times heavier than H^+ . Combining our results with earlier observations, we propose an explanation for the observed asymmetries. Since the MESSENGER spacecraft spent most of its orbital time sunward of the statistical NMNL [Poh *et al.* 2017], the plasma convecting sunward from a NMNL farther downtail would undergo gradient-curvature drift in addition to the $\mathbf{E} \times \mathbf{B}$ drift imposed by the cross-tail electric field. The ions (i.e., H^+ , Na^+ , and O^+) drift duskward (premidnight) into the inner current sheet to energies of 1–5 keV [Zurbuchen *et al.*, 2011], while the electrons drift dawnward. Furthermore, Delcourt [2013] show that cold Na^+ and O^+ originating from Mercury's cusp can be accelerated due to centrifugal drift and undergo nonadiabatic Speiser-type orbits moving preferentially into the duskside inner current sheet. This process is similar to the ionospheric cusp outflow of oxygen ions moving into the plasma sheet at Earth. The mass loading of energetic heavy ions from the NMNL and cusp increases the thermal plasma pressure duskside of the current sheet, resulting in stretching (weaker B_z) and thinning of the duskside current sheet (Figure 5, bottom right).

Consequently, this leads to the question on the effects of mass loading on current sheet dynamics at Mercury's duskside inner tail current sheet. Specifically, does the thinning of Mercury's dusk side inner tail current sheet due to higher amount of heavy ions make it unstable to magnetic reconnection planetward of the NMNL? At Earth, studies on reconnection-related processes (e.g., near-Earth reconnection signatures [Eastwood *et al.*, 2010; Nagai *et al.*, 2013]) and structures (e.g., plasmoids/traveling compression regions [Slavin *et al.*, 1985; Imber *et al.*, 2011] and dipolarization fronts [Liu *et al.*, 2013]) observed higher occurrence rates toward dusk, which strongly indicates that reconnection is more likely to occur duskward of the current sheet. The asymmetry of O^+ presence in the terrestrial magnetotail leads us to question if there is any relationship between heavy ions and reconnection.

The effect of O^+ on reconnection in Earth's plasma sheet remains controversial within the scientific community. Baker *et al.* [1982] first argued that the asymmetric distribution of O^+ in Earth's plasma sheet may increase the growth of tearing mode instability, resulting in higher reconnection rate toward dusk. On the other hand, Shay and Swisdak [2004] concluded from their three-fluid simulation that the presence of O^+ can slow the reconnection rate since O^+ , being a heavier ion, reduces the inflow Alfvén speed. Kinetic simulations have also shown slower dipolarization fronts speed [Liang *et al.*, 2016] and reduced frequency of secondary islands in reconnection region [Karimabadi *et al.*, 2011] due to nonlinear effects. Recently, multifluid simulations by Zhang *et al.* [2016] suggested that earthward traveling flux ropes are more likely to form in the presence of ionospheric O^+ as it can reduce the reconnection rate of X lines closer to Earth, leading to the formation of the dominant X line (i.e., NENL) farther downtail.

Since Earth's and Mercury's magnetospheres have similar magnetic structure, higher occurrence rate of reconnection is expected at the stretched, duskward current sheet from the observed asymmetry of hot Na^+ [Raines *et al.*, 2013; Gershman *et al.*, 2014] and the effect might be stronger at Mercury since Na^+ is typically the dominant ion species. Higher occurrence rates of magnetic reconnection by-products (e.g., flux ropes and dipolarization fronts) are also expected at the duskside current sheet. However, earlier studies by DiBraccio *et al.* [2015a] observed no systematic asymmetry in the occurrence rate of plasmoids. More recently, Sun *et al.* [2016] analyzed magnetic field data during MESSENGER orbital time period similar to earlier studies and observed a dawnward increase in the occurrence rate of plasmoids and reconnection fronts. Lindsay *et al.* [2016] also reported more X-ray fluorescence events induced by precipitating energetic electrons from reconnection on the dawnside of Mercury's surface. These observations suggest that reconnection preferentially occurs dawnside of Mercury's current sheet [Sun *et al.*, 2016]. Furthermore, the idea of dawnward preference in magnetotail reconnection supports our observation of a dawnward asymmetric magnetic flux pileup region, which is caused by the braking of dipolarized, planetward traveling flux tubes that had reconnected at an X line farther downtail.

Combined with earlier indirect observations of magnetic reconnection, our results demonstrated that the effects of heavy ions (primarily Na^+) on magnetic reconnection at Mercury's magnetotail seem to be less controversial than at Earth. Higher amount of heavy ions in the duskside current sheet does not make it unstable to reconnection. In fact, heavy ions lower the reconnection rate at the duskside current sheet, which means that the dawnside current sheet has a higher occurrence of reconnection and reconnection-related dynamics than the duskside. Despite having an opposite asymmetry pattern, the asymmetry in B_z , current sheet thickness, and β_{CS} is also consistent with the dawnward preference in reconnection. Higher occurrence of reconnection in the dawnside current sheet sends dipolarized flux tubes toward the dawnside of the inner magnetotail. This process thickens the postmidnight (dawnside) current sheet in Mercury's inner tail region while mass loading of H^+ and heavy ions (e.g., Na^+ and O^+) continues to thin the premidnight (duskside) current sheet, as shown in Figure 5. The mechanism responsible for the asymmetries observed at Mercury appears to be very different from that of Earth, and we think that the differential thickening and thinning of the postmidnight and premidnight current sheet could explain our observation of Mercury's asymmetry being stronger than Earth's. At Earth, the effects of earthward propagating dipolarized flux tubes or dipolarization events are removed when averaged over long time period. However, due to the small size of Mercury's magnetosphere, the effects of the positive B_z (i.e., thickening of the current sheet) from the dipolarization events may be significant as suggested in this study.

4.2. Observation of Mercury's Substorm Current Wedge

An enhancement of B_z around midnight in the $-1.4 R_M > X_{\text{MSM}} > -1.7 R_M$ downtail region (Figure 2, first panel) is observed in our results, which strongly suggest the direct measurement of substorm current wedge formation at Mercury. Due to the lack of in situ observations, substorm current wedge in other planetary magnetotails (Mercury's in particular) is not well understood and has not been observed directly. However, the presence of a Hermean SCW has been observed in global hybrid simulations [e.g., *Janhunen and Kallio, 2004*]. Substorms and other substorm-related processes, such as loading and unloading of magnetic flux in the tail lobe, dipolarization [*Sundberg et al., 2012; Sun et al., 2015, 2016*], and plasmoid ejection [*Slavin et al., 2010, 2012; DiBraccio et al., 2015a*] have all been observed at Mercury in the MESSENGER data. These are indirect evidence of the presence of a SCW at Mercury.

Substorms at Earth had been extensively studied since its discovery by ground-based [*Akasofu, 1964*] and space-based [*McPherron et al., 1973; Hesse and Birn, 1991; Shiokawa et al., 1997*] measurements. Many theories had been proposed to explain the substorm process at Earth, but it is now widely accepted that the substorm growth phase begins when the dayside reconnection rate exceeds the nightside reconnection rate, resulting in the building up of magnetic flux in the tail lobes and stretching of magnetotail field lines. Substorm expansion phase is initiated when a sudden burst of reconnection (i.e., unloading of lobe magnetic flux) occurs in the plasma sheet and launches an Alfvénic flow burst, carrying dipolarized flux tubes toward and away from Earth. It is the braking of the earthward bursty bulk flows (BBFs) due to the tailward pressure gradient force and diversion of plasma flow as it approaches the strongly dipolar, high- β inner magnetotail that creates the substorm current wedge (see *Kepko et al. [2015]* for complete review).

At Earth, BBFs are rarely observed inside of $9 R_E$ [*McPherron et al., 2011*] and the probability of observing these high-speed flows exceeding 400 km/s decreases sharply at $X_{\text{GSM}} \approx -13 R_E$ [e.g., *Shiokawa et al., 1997*], which is consistent with the location of the SCW at $\approx 9-13 R_E$. Scaling of the terrestrial SCW location with a factor of 8 [*Ogilvie et al., 1977*], the location of Mercury's SCW is expected to be $X'_{\text{MSM}} \approx -1.1$ to $-1.7 R_M$. An earlier study on Mercury's substorm activity [*Sun et al., 2015*] also reported observations of substorms growth and expansion phase within $X'_{\text{MSM}} > -1.7 R_M$. Since the magnetic flux pileup in our results is observed between $X'_{\text{MSM}} = -1.4 R_M$ and $-1.7 R_M$, our observation of the SCW in Mercury's inner tail region corroborates with terrestrial expectations and earlier MESSENGER observation of Mercury's substorm activity.

Using a simple line current model, we can estimate the total SCW current I_{SCW} required to produce the observed dawn-dusk profile of the detrended positive magnetic field perturbation δB_z due to the SCW (red line in Figure 3a). Figure 6 shows the three-dimensional, meridional, and equatorial views of the model setup. In this model, the SCW is modeled as four infinitely thin line current segments. The braking of the fast planetward plasma flow results in a dawnward current (Segment 1) perpendicular to the magnetic field in the

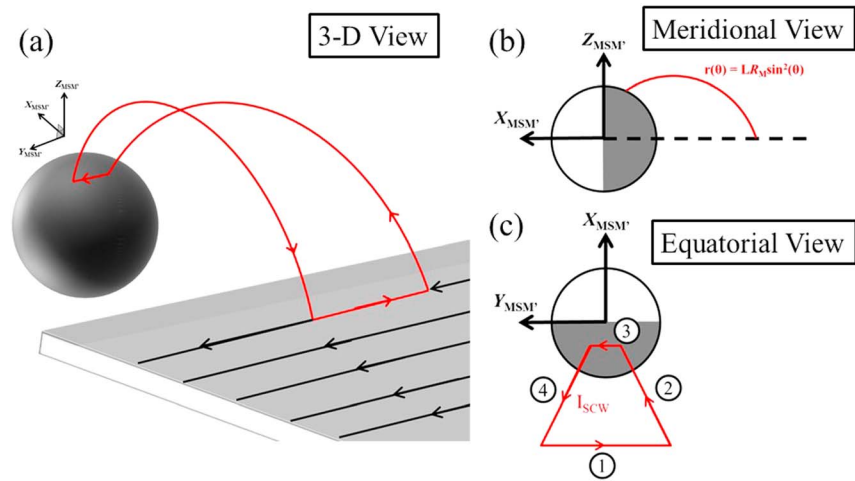


Figure 6. Schematic illustrations of Mercury's substorm current wedge, in (a) three-dimensional, (b) meridional, and (c) equatorial views, using a simple line current model. Black arrows represent the cross-tail current direction in Mercury's current sheet, while red arrows represent the path and direction of the current flow in the substorm current wedge. The substorm current wedge is modeled using four infinitely thin line current segments. The currents in Segments 1 and 3 flow perpendicular to the magnetic field, while currents in Segments 2 and 4 flow parallel to the magnetic field. A dipole magnetic field is used to model the magnetic field lines in Segments 2 and 4. The magnetic field perturbation δB_Z is calculated by adding the magnetic field contribution from each line current segment, which is determined using the Biot-Savart law.

equatorial region, which is opposite to the duskward cross-tail current. At the edge of the current wedge, the current is diverted and flows along the magnetic field toward Mercury. The dipole magnetic field is used to model the magnetic field lines in Segments 2 and 4. The lack of an ionosphere at Mercury means that the current closure mechanism is different from that at Earth. Through analysis and modeling of the MESSENGER magnetometer data, Anderson *et al.* [2014] identified and modeled the Region 1 field-aligned currents (FACs) at Mercury. Their analysis revealed field-aligned currents with intensities of tens of kiloamperes flowing radially downward on the dawnside then along the surface of its highly conductive core and radially upward on the duskside of the auroral oval through Mercury's resistive regolith (i.e., Region 1 currents). This indicates the possibility of similar current closure mechanism for FAC associated with the SCW as shown in Segment 3 of Figure 6c.

Using the Biot-Savart law, we calculated the magnetic field contributions at $X'_{MSM} = -1.55 R_M$ from the four segments of the model SCW as a function of Y'_{MSM} . Not shown here, the model includes magnetic field perturbations from both hemispheres of the substorm current wedge. We then fitted the model dawn-dusk profile of δB_Z to the observed profile, with I_{SCW} , relative distance between line current in Segment 1 and the point $X'_{MSM} = -1.55 R_M$, and width of the SCW as free parameters. We also shifted the peak of the model profile dawnward to obtain a better fit. Figure 7 shows the model (black) and the observed (red) dawn-dusk profile of δB_Z due to the SCW. We determined that a current of ≈ 11 kA in each hemisphere of the substorm current wedge is required to produce the observed dawn-dusk profile of δB_Z ; our estimated SCW current is ≈ 25 –50% of the typical value for Region 1 currents (≈ 20 –40 kA) [Anderson *et al.*, 2014]. As shown in Figure 7, the δB_Z profile of the model substorm current wedge fits perfectly to the observed profile between the midnight meridian and $Y'_{MSM} = -0.5 R_M$, with the center of the current wedge at $Y'_{MSM} \approx 0.15 R_M$. Our fitting results further suggest that there is an obvious asymmetry in the agreement between model and observation and the reason for this asymmetry feature remains a question. The model deviates from the observations with increasing distance from the center of the SCW, which suggest the presence of additional current systems at the edge of the current wedge not accounted for in this simple line current model.

We calculate the electric potential Φ across the SCW from the equation $\Phi = V_x B_z \Delta y$, where Δy is the length of the pileup region in the Y'_{MSM} direction, B_z is the Z component of the average magnetic field vector, and V_x is the antisunward component (i.e., X'_{MSM}) of BBF flow velocity before braking. The view direction of FIPS when MESSENGER traverses the current sheet is in the north-south direction. Hence, FIPS cannot measure plasma

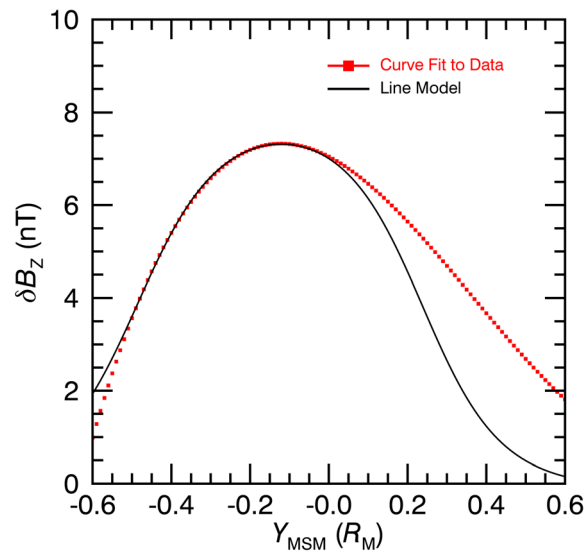


Figure 7. Dawn-dusk profile of magnetic field perturbation δB_z calculated from the line current model (black line) and the cubic polynomial fit to the observed increase in B_z in Figure 3a (red dashed line). The line current model profile is fitted to the observed B_z profile with I_{SCW} , relative distance between line current in Segment 1 (Figure 6c) and the point $X'_{MSM} = -1.55 R_M$, and width of the SCW as free parameters. The peak of the line current model profile is shifted downward to obtain a better fit. Analysis shows good agreements between model and observation between midnight meridian and $Y_{MSM} = -0.5 R_M$ with the center of the substorm current wedge at $Y_{MSM} \approx -0.15 R_M$. Inconsistency between model and observations at the edge of the SCW suggests the presence of additional current systems in the SCW not taken into account in this simple line current model.

earthward traveling flux tubes that had reconnected farther downtail [Shiokawa *et al.*, 1997]. Therefore, the higher magnetic flux in the postmidnight flux pileup region also suggests a dawnward preference in the occurrence of magnetic reconnection. This result has very important implications on the nature of magnetic reconnection in the inner tail region of Mercury's magnetotail. For example, Sun *et al.* [2016] analyzed 86 dipolarization fronts identified in Mercury's plasma sheet. They concluded that there is a dawnward preference in occurrence of reconnection fronts observed at Mercury (Figure 3b), which has similar asymmetry pattern as our B_z results. This further provides support for our explanation of the observed asymmetries mentioned in earlier sections, where the difference in stretching (mass loading of ions) and thickening (dipolarized flux tube) of Mercury's current sheet may explain the asymmetries in B_z and current sheet thickness.

5. Conclusions

In this study, we have shown how Mercury couples with its nightside magnetosphere through mass, momentum, and energy transport in the magnetotail. We presented MESSENGER observations of a dawn-dusk asymmetry in B_z , β_{CS} , and the thickness of Mercury's current sheet. They are consistent with MHD stress balance and similar to the magnetotail asymmetries observed at Earth. It is found that B_z , β_{CS} , and thickness are lower, higher, and thinner, respectively, on the duskside than the dawnside current sheet. We propose that the asymmetry observed in our study is the result of mass loading of Na^+ into the duskside current sheet from the NMNL and cusp. This mass loading leads to closed flux tubes stretching and a thinner duskside than dawnside current sheet. Recent studies of reconnection-related phenomenon in Mercury's inner tail region suggest that reconnection preferentially occur dawnside of its current sheet [Sun *et al.*, 2016]. Our analysis shows that B_z is higher in the dawnside magnetic pileup region, which also supports higher reconnection

velocity in the X direction. Since the BBFs are accelerated to local Alfvén speed at the outflow region of the reconnection X line, we can assume $V_x \approx 465$ km/s, which is the average Alfvén velocity in the plasma sheet calculated measured in Mercury's plasma sheet by MESSENGER [DiBraccio *et al.*, 2015a]. Using the values of $\Delta y \approx 0.8 R_M$ and $B_z \approx 10$ nT, we estimate the potential across the substorm current wedge to be ≈ 9 kV. We further calculate the electrical conductance of Mercury's surface necessary to close the current to be ≈ 1.2 S. Our estimated value of Mercury's surface conductance from the SCW agrees with the net electrical conductance of ≈ 1 S calculated from Mercury's Birkeland current [Anderson *et al.*, 2014]. This supports our idea of a similar current closure mechanism between Mercury's substorm current wedge and the field-aligned Region 1 currents. Despite the absence of an ionosphere, it is very likely that the current in Mercury's substorm current wedge closed radially through resistive regolith then on the surface of Mercury's highly conductive iron core [see Anderson *et al.*, 2014, Figure 4a].

Another interesting result of our analysis is the higher magnetic flux in the postmidnight magnetic flux pileup region (see Figure 3a). As mentioned earlier, the pileup region (or SCW) is caused by the braking of dipolarized

occurrence in the dawnside current sheet but at larger downstream distances than directly sampled by MESSENGER. The thicker dawnside current sheet found in our study at MESSENGER orbit requires a source of sunward closed magnetic flux, which is stronger on the dawnside. Accidentally, our observed asymmetry in B_z sunward of the NMNL is consistent with the higher occurrence of magnetic reconnection reported by Sun *et al.* [2016] on the basis of the occurrence of dipolarization fronts and flux ropes. These effects driven by reconnection farther down the tail enhance the dawn-dusk asymmetry already present due to mass loading of Na^+ in the duskside inner tail region. Despite many similarities in Mercury's and Earth's magnetotail, it appears that the mechanisms for magnetotail asymmetry at Mercury are different from that at Earth due to differences in the internal plasma composition.

We also report the direct measurement of substorm current wedge formation in Mercury's inner magnetotail. Using a simple line current model, we estimated the total SCW current associated with the observed magnetic field perturbations to be ≈ 11 kA. We also calculated the potential across the substorm current wedge to be ≈ 9 kV and an integrated conductance of ≈ 1.2 S to close the current in the current wedge. Our inferred conductance value for the lumped crust-outer core current closure path is similar to that determined for the field-aligned Region 1 currents [Anderson *et al.*, 2014]. Therefore, our results are consistent with Mercury's regolith being electrically conductive enough to support the radial closure of the current wedge field-aligned currents, generated from braking and diversion of fast plasma flows, through the regolith. The current then closes across the surface of Mercury's highly conductive core near the latitude of the nightside auroral oval.

Several important questions on the nature of current sheet dawn-dusk asymmetry, magnetospheric substorm, and magnetotail reconnection at Mercury surfaced from this study. Specifically, (1) are there any dawn-dusk asymmetries in the location and properties of the NMNL? (2) Does the observed asymmetry in internal plasma composition of Mercury's current sheet have any effect on the large-scale reconnection dynamics (e.g., formation and evolution of flux ropes and BBFs) as proposed by terrestrial studies? (3) At what downtail distance does the high-speed plasma flow braking and fraction of the incident flow is diverted about the planet? Is the amount of braking and surface impact consistent with the substorm current wedge intensity determined here using magnetic field measurements?

Looking further into the future, analysis of magnetic field and plasma measurements from the upcoming European Space Agency's Bepi-Colombo mission will take our understanding of Mercury's magnetospheric dynamics to the next level. The reconnaissance carried out by MESSENGER mission has generated many more fundamental questions than it answered. The Bepi-Colombo mission, which consists of two orbiters (Mercury Planetary Orbiter and Mercury Magnetospheric Orbiter) with apogees of $X'_{\text{MSM}} \approx -1.6 R_M$ and $-5 R_M$, respectively, will allow simultaneous two-point observations within the magnetosphere and with one spacecraft in the solar wind at aphelion and the other close to Mercury, but in the magnetosphere. These advances in our observational data sets will lead to great improvements in our understanding of magnetospheric dynamics at Mercury.

Acknowledgments

All data analyzed in this paper are archived with the NASA Planetary Data System (<https://pds.nasa.gov/>). Support was provided by NASA Discovery Data Analysis Program grants NNX15K88G and NNX15AL01G, Heliophysics Supporting Research NNX15AJ68G, Living with a Star NNX16AJ67G, and Solar System Workings Program grant NNX15AH28G to the University of Michigan. D.J.G and G.A.D were supported by NASA ROSES grant NNX16AJ05G. S.I.M acknowledges the support of the Leverhulme Trust. W.J.S is funded by National Postdoctoral Program for Innovative Talents (BX201600158) and China Postdoctoral Science Foundation (2016M600124).

References

- Akasofu, S.-I. (1964), The development of the auroral substorm, *Planet. Space Sci.*, *12*(4), 273–282, doi:10.1016/0032-0633(64)90151-5.
- Alexeev, I. I., *et al.* (2010), Mercury's magnetospheric magnetic field after the first two MESSENGER flybys, *Icarus*, *209*, 23–39, doi:10.1016/j.icarus.2010.01.024.
- Anderson, B. J., M. H. Acuña, D. A. Lohr, J. Scheifele, A. Raval, H. Korth, and J. A. Slavin (2007), The Magnetometer instrument on MESSENGER, *Space Sci. Rev.*, *131*(1–4), 417–450, doi:10.1007/s11214-007-9246-7.
- Anderson, B. J., C. L. Johnson, H. Korth, M. E. Purucker, R. M. Winslow, J. A. Slavin, S. C. Solomon, R. L. McNutt Jr., J. M. Raines, and T. H. Zurbuchen (2011), The global magnetic field of Mercury from MESSENGER orbital observations, *Science*, *333*(6051), 1859–1862, doi:10.1126/science.1211001.
- Anderson, B. J., C. L. Johnson, H. Korth, J. A. Slavin, R. M. Winslow, R. J. Phillips, S. C. Solomon, and R. L. McNutt Jr. (2014), Steady-state field-aligned currents at Mercury, *Geophys. Res. Lett.*, *41*, 7444–7452, doi:10.1002/2014GL061677.
- Andrews, G. B., *et al.* (2007), The Energetic Particle and Plasma spectrometer instrument on the MESSENGER spacecraft, *Space Sci. Rev.*, *131*(1–4), 523–556, doi:10.1007/s11214-007-9272-5.
- Arridge, C. S., M. Kane, N. Sergis, K. K. Khurana, and C. M. Jackman (2015), Sources of local time asymmetries in magnetodiscs, *Space Sci. Rev.*, *187*(1), 301–333, doi:10.1007/s11214-015-0145-z.
- Artemyev, A. V., A. A. Petrukovich, R. Nakamura, and L. M. Zelenyi (2011), Cluster statistics of thin current sheets in the Earth magnetotail: Specifics of the dawn flank, proton temperature profiles and electrostatic effects, *J. Geophys. Res.*, *116*, A09233, doi:10.1029/2011JA016801.
- Artemyev, A. V., V. Angelopoulos, and A. Runov (2016), On the radial force balance in the quiet time magnetotail current sheet, *J. Geophys. Res. Space Physics*, *121*, 4017–4026, doi:10.1002/2016JA022480.
- Baker, D. N., E. W. Hones, D. T. Young, and J. Birn (1982), The possible role of ionospheric oxygen in the initiation and development of plasma sheet instabilities, *Geophys. Res. Lett.*, *9*, 1337–1340, doi:10.1029/GL0091012p01337.

- Baumjohann, W., G. Paschmann, and H. Lühr (1990), Characteristics of high-speed ion flows in the plasma sheet, *J. Geophys. Res.*, *95*, 3801–3809, doi:10.1029/JA095iA04p03801.
- Baumjohann, W., M. Hesse, S. Kokubun, T. Mukai, T. Nagai, and A. A. Petrukovich (1999), Substorm dipolarization and recovery, *J. Geophys. Res.*, *104*, 24995–25000, doi:10.1029/1999JA900282.
- Bunce, E. J., and S. W. H. Cowley (2001), Local time asymmetry of the equatorial current sheet in Jupiter's magnetosphere, *Planet. Space Sci.*, *49*(3–4), 261–274, doi:10.1016/S0032-0633(00)00147-1.
- Delcourt, D. C. (2013), On the supply of heavy planetary material to the magnetotail of Mercury, *Ann. Geophys.*, *31*, 1673–1679, doi:10.5194/angeo-31-1673-2013.
- DiBraccio, G. A., J. A. Slavin, S. A. Boardsen, B. J. Anderson, H. Korth, T. H. Zurbuchen, J. M. Raines, D. N. Baker, R. L. McNutt Jr., and S. C. Solomon (2013), MESSENGER observations of magnetopause structure and dynamics at Mercury, *J. Geophys. Res. Space Physics*, *118*, 997–1008, doi:10.1002/jgra.50123.
- DiBraccio, G. A., et al. (2015a), MESSENGER observations of flux ropes in Mercury's magnetotail, *Planet. Space Sci.*, *115*, 77–89, doi:10.1016/j.pss.2014.12.016.
- DiBraccio, G. A., et al. (2015b), Magnetotail dynamics at Mars: Initial MAVEN observations, *Geophys. Res. Lett.*, *42*, 8828–8837, doi:10.1002/2015GL065248.
- DiBraccio, G. A., et al. (2017), MAVEN observations of tail current sheet flapping at Mars, *J. Geophys. Res. Space Physics*, *122*, doi:10.1002/2016JA023488.
- Eastwood, J. P., T. D. Phan, M. Øieroset, and M. A. Shay (2010), Average properties of the magnetic reconnection ion diffusion region in the Earth's magnetotail: The 2001–2005 Cluster observations and comparison with simulations, *J. Geophys. Res.*, *115*, A08215, doi:10.1029/2009JA014962.
- Fairfield, D. H. (1979), On the average configuration of the geomagnetic tail, *J. Geophys. Res.*, *84*, 1950–1958, doi:10.1029/JA084iA05p01950.
- Fairfield, D. H., R. P. Lepping, E. W. Hones Jr., S. J. Bame, and J. R. Asbridge (1981), Simultaneous measurements of magnetotail dynamics by IMP spacecraft, *J. Geophys. Res.*, *86*, 1396–1414.
- Genestreti, K. J., S. A. Fuselier, J. Goldstein, T. Nagai, and J. P. Eastwood (2014), The location and rate of occurrence of near-Earth magnetotail reconnection as observed by Cluster and Geotail, *J. Atmos. Sol. Terr. Phys.*, *121*, Part A, 98–109.
- Gershman, D. J., J. A. Slavin, J. M. Raines, T. H. Zurbuchen, B. J. Anderson, H. Korth, D. N. Baker, and S. C. Solomon (2014), Ion kinetic properties in Mercury's pre-midnight plasma sheet, *Geophys. Res. Lett.*, *41*, 5740–5747, doi:10.1002/2014GL060468.
- Harris, E. G. (1962), On a plasma sheath separating regions of oppositely directed magnetic field, *Nuovo Cimento*, *23*, 115–121.
- Hesse, M., and J. Birn (1991), On dipolarization and its relation to the substorm current wedge, *J. Geophys. Res.*, *96*, 19,417–19,426, doi:10.1029/91JA01953.
- Imber, S. M., J. A. Slavin, H. U. Auster, and V. Angelopoulos (2011), A THEMIS survey of flux ropes and traveling compression regions: Location of the near-Earth reconnection site during solar minimum, *J. Geophys. Res.*, *116*, A02201, doi:10.1029/2010JA016026.
- Janhunen, P., and E. Kallio (2004), Surface conductivity of Mercury provides current closure and may affect magnetospheric symmetry, *Ann. Geophys.*, *22*, 1829–1837, doi:10.5194/angeo-22-1829-2004.
- Karimabadi, H., V. Roytershteyn, C. G. Mouikis, L. M. Kistler, and W. Daughton (2011), Flushing effect in reconnection: Effects of minority species of oxygen ions, *Planet. Space Sci.*, *59*(7), 526–536.
- Kepko, L., et al. (2015), Substorm current wedge revisited, *Space Sci. Rev.*, *190*, 1, doi:10.1007/s11214-014-0124-9.
- Liang, H., M. Ashour-Abdalla, G. Lapenta, and R. J. Walker (2016), Oxygen impacts on dipolarization fronts and reconnection rate, *J. Geophys. Res. Space Physics*, *121*, 1148–1166, doi:10.1002/2015JA021747.
- Lindsay, S. T., M. K. James, E. J. Bunce, S. M. Imber, H. Korth, A. Martindale, and T. K. Yeoman (2016), MESSENGER X-ray observations of magnetosphere-surface interaction on the nightside of Mercury, *Planet. Space Sci.*, *125*, 72–79, doi:10.1016/j.pss.2016.03.005.
- Liu, J., V. Angelopoulos, A. Runov, and X.-Z. Zhou (2013), On the current sheets surrounding dipolarizing flux bundles in the magnetotail: The case for wedgelets, *J. Geophys. Res. Space Physics*, *118*, 2000–2020, doi:10.1002/jgra.50092.
- McPherron, R. L., C. T. Russell, and M. P. Aubry (1973), Satellite studies of magnetospheric substorms on August 15, 1968: 9. Phenomenological model for substorms, *J. Geophys. Res.*, *78*, 3131–3149, doi:10.1029/JA078i016p03131.
- McPherron, R. L., T.-S. Hsu, J. Kissinger, X. Chu, and V. Angelopoulos (2011), Characteristics of plasma flows at the inner edge of the plasma sheet, *J. Geophys. Res.*, *116*, A00133, doi:10.1029/2010JA015923.
- Nagai, T., I. Shinohara, S. Zenitani, R. Nakamura, T. K. M. Nakamura, M. Fujimoto, Y. Saito, and T. Mukai (2013), Three-dimensional structure of magnetic reconnection in the magnetotail from Geotail observations, *J. Geophys. Res. Space Physics*, *118*, 1667–1678, doi:10.1002/jgra.50247.
- Ogilvie, K. W., J. D. Scudder, V. M. Vasyliunas, R. E. Hartle, and G. L. Siscoe (1977), Observations at the planet Mercury by the plasma electron experiment: Mariner 10, *J. Geophys. Res.*, *82*, 1807–1824, doi:10.1029/JA082i013p01807.
- Ohtani, S., M. Nosé, S. P. Christon, and A. T. Y. Lui (2011), Energetic O⁺ and H⁺ ions in the plasma sheet: Implications for the transport of ionospheric ions, *J. Geophys. Res.*, *116*, A10211, doi:10.1029/2011JA016532.
- Peterson, W. K., R. D. Sharp, E. G. Shelley, R. G. Johnson, and H. Balsiger (1981), Energetic ion composition of the plasma sheet, *J. Geophys. Res.*, *86*, 761–767, doi:10.1029/JA086iA02p00761.
- Petrukovich, A. A., A. V. Artemyev, H. V. Malova, V. Y. Popov, R. Nakamura, and L. M. Zelenyi (2011), Embedded current sheets in the Earth's magnetotail, *J. Geophys. Res.*, *116*, A00125, doi:10.1029/2010JA015749.
- Poh, G., J. A. Slavin, X. Jia, J. M. Raines, S. M. Imber, W.-J. Sun, D. J. Gershman, G. A. DiBraccio, K. J. Genestreti, and A. W. Smith (2017), Mercury's cross-tail current sheet: Structure, X-line location and stress balance, *Geophys. Res. Lett.*, *44*, 678–686, doi:10.1002/2016GL071612.
- Pritchett, P. L., and F. V. Coroniti (1992), Formation and stability of the self-consistent one-dimensional tail current sheet, *J. Geophys. Res.*, *97*16, 773.
- Raines, J. M., et al. (2013), Distribution and compositional variations of plasma ions in Mercury's space environment: The first three Mercury years of MESSENGER observations, *J. Geophys. Res. Space Physics*, *118*, 1604–1619, doi:10.1029/2012JA018073.
- Rong, Z. J., W. X. Wan, C. Shen, X. Li, M. W. Dunlop, A. A. Petrukovich, T. L. Zhang, and E. Lucek (2011), Statistical survey on the magnetic structure in magnetotail current sheets, *J. Geophys. Res.*, *116*, A09218, doi:10.1029/2011JA016489.
- Rong, Z. J., S. Barabash, G. Stenborg, Y. Futaana, T. L. Zhang, W. X. Wan, Y. Wei, X. D. Wang, L. H. Chai, and J. Zhong (2015), The flapping motion of the Venusian magnetotail: Venus Express observations, *J. Geophys. Res. Space Physics*, *120*, 5593–5602, doi:10.1002/2015JA021317.
- Shay, M. A., and M. Swisdak (2004), Three-species collisionless reconnection: Effect of O⁺ on magnetotail reconnection, *Phys. Rev. Lett.*, *93*, 175001, doi:10.1103/PhysRevLett.93.175001.
- Shiokawa, K., W. Baumjohann, and G. Haerendel (1997), Braking of high-speed flows in the near-Earth tail, *Geophys. Res. Lett.*, *24*, 1179–1182, doi:10.1029/97GL01062.

- Slavin, J. A., and R. E. Holzer (1979), The effect of erosion on the solar wind stand-off distance at Mercury, *J. Geophys. Res.*, *84*, 2076–2082, doi:10.1029/JA084iA05p02076.
- Slavin, J. A., E. J. Smith, D. G. Sibeck, D. N. Baker, R. D. Zwickl, and S.-I. Akasofu (1985), An ISEE 3 study of average and substorm conditions in the distant magnetotail, *J. Geophys. Res.*, *90*, 10,875–10,895.
- Slavin, J. A., et al. (2009), MESSENGER observations of magnetic reconnection in Mercury's magnetosphere, *Science*, *324*, 606–610, doi:10.1126/science.1172011.
- Slavin, J. A., et al. (2010), MESSENGER observations of extreme loading and unloading of Mercury's magnetic tail, *Science*, *329*, 665–668, doi:10.1126/science.1188067.
- Slavin, J. A., et al. (2012), MESSENGER and Mariner 10 flyby observations of magnetotail structure and dynamics at Mercury, *J. Geophys. Res.*, *117*, A01215, doi:10.1029/2011JA016900.
- Smith, A. W., C. M. Jackman, and M. F. Thomsen (2016), Magnetic reconnection in Saturn's magnetotail: A comprehensive magnetic field survey, *J. Geophys. Res. Space Physics*, *121*, 2984–3005, doi:10.1002/2015JA022005.
- Sun, W.-J., et al. (2015), MESSENGER observations of magnetospheric substorm activity in Mercury's near magnetotail, *Geophys. Res. Lett.*, *42*, 3692–3699, doi:10.1002/2015GL064052.
- Sun, W. J., S. Y. Fu, J. A. Slavin, J. M. Raines, Q. G. Zong, G. K. Poh, and T. H. Zurbuchen (2016), Spatial distribution of Mercury's flux ropes and reconnection fronts: MESSENGER observations, *J. Geophys. Res. Space Physics*, *121*, 7590–7607, doi:10.1002/2016JA022787.
- Sundberg, T., et al. (2012), MESSENGER observations of dipolarization events in Mercury's magnetotail, *J. Geophys. Res.*, *117*, A00M03, doi:10.1029/2012JA017756.
- Tsyganenko, N. A. (1995), Modeling the Earth's magnetospheric magnetic field confined within a realistic magnetopause, *J. Geophys. Res.*, *100*, 5599–5612, doi:10.1029/94JA03193.
- Vasko, I. Y., A. A. Petrukovich, A. V. Artemyev, R. Nakamura, and L. M. Zelenyi (2015), Earth's distant magnetotail current sheet near and beyond lunar orbit, *J. Geophys. Res. Space Physics*, *120*, 8663–8680, doi:10.1002/2015JA021633.
- Volwerk, M., et al. (2013), Comparative magnetotail flapping: An overview of selected events at Earth, Jupiter and Saturn, *Ann. Geophys.*, *31*, 817–833, doi:10.5194/angeo-31-817-2013.
- Walsh, A. P., et al. (2017), Dawn-dusk asymmetries in the coupled solar wind-magnetosphere-ionosphere system: A review, *Ann. Geophys.*, *32*, 705–737, doi:10.5194/angeo-32-705-2014.
- Wang, C.-P., L. R. Lyons, M. W. Chen, and F. R. Toffoletto (2004), Modeling the transition of the inner plasma sheet from weak to enhanced convection, *J. Geophys. Res.*, *109*, A12202, doi:10.1029/2004JA010591.
- Winslow, R. M., B. J. Anderson, C. L. Johnson, J. A. Slavin, H. Korth, M. E. Purucker, D. N. Baker, and S. C. Solomon (2013), Mercury's magnetopause and bow shock from MESSENGER Magnetometer observations, *J. Geophys. Res. Space Physics*, *118*, 2213–2227, doi:10.1002/jgra.50237.
- Zhang, B., O. J. Brambles, W. Lotko, J. E. Ouellette, and J. G. Lyon (2016), The role of ionospheric O⁺ outflow in the generation of earthward propagating plasmoids, *J. Geophys. Res. Space Physics*, *121*, 1425–1435, doi:10.1002/2015JA021667.
- Zurbuchen, T. H., et al. (2011), MESSENGER observations of the spatial distribution of planetary ions near Mercury, *Science*, *333*, 1862–1865, doi:10.1126/science.1211302.